

New Results on Short-Range Correlations in Nuclei

Nadia Fomin¹, Douglas Higinbotham², Misak Sargsian³ and Patricia Solvignon^{4*}

¹ University of Tennessee, Knoxville, TN 37996

² Jefferson Lab, Newport News, VA, 23606

³ Florida International University, Miami, FL 33199

⁴ University of New Hampshire, Durham, NH 03824

Annu. Rev. Nucl. Part. 2017.67:129-59
2017. AA:1–32

This article's doi:
10.1146/annurev-nucl-102115-044939

Copyright © 2017 by Annual Reviews.
All rights reserved

Keywords

Short-range nucleon correlations, high energy electron nucleus scattering, deep inelastic nuclear scattering, super-fast quarks

Abstract

Nuclear dynamics at short distances is one of the most fascinating topics of strong interaction physics. The physics of it is closely related to the understanding the role of the QCD in generating nuclear force at short distances as well as understanding the dynamics of the super-dense cold nuclear matter relevant to the interior of neutron stars. With an emergence of high energy electron and proton beams there is a significant recent progress in high energy nuclear scattering experiments aimed at studies of short-range structure of nuclei. This in turn stimulated new theoretical studies resulting in the observation of several new phenomena specific to the short range structure of nuclei. In this work we review recent theoretical and experimental progress in studies of short-range correlations in nuclei and their importance for advancing our understanding of the dynamics of nuclear interactions at small distances.

1. Introduction

Nuclear Physics at Short Distances: One of the outstanding issues in contemporary nuclear physics is understanding the role of Quantum Chromodynamics (QCD) in generating the nuclear forces. There has been significant progress in understanding the medium to long range ($\gtrsim 1.2$ fm) part of the nuclear forces in terms of effective field theories in which pion exchange forces are constructed to satisfy QCD symmetries and the dynamics in which pion is a Goldstone boson of the spontaneously broken chiral symmetry (for recent review see Ref. (1)). However, one of the challenging and less understood domains of nuclear forces is that of intermediate to short distances ($\lesssim 1.2$ fm). This is the domain of the transition from baryonic to quark-gluon degrees of freedom where one expects a host of new phenomena inherent to QCD dynamics which are not visible to long range nuclear forces. These include chiral symmetry, quark interchanges, gluon dynamics, hidden color states, among others. One of the most fascinating short distance phenomena is the practically unexplored dynamics of the nuclear repulsive core. We owe our existence literally to the nuclear core, without which nuclei will collapse to sizes $\leq 0.3 - 0.4$ fm, followed by the onset of quark-gluon degrees of freedom and restoration of chiral symmetry with rather unimaginable consequences for the order of the universe we know.

Within above mentioned effective field theories the short-range nuclear forces are described through the effective contact interactions whose internal structure is invisible in low energy processes. However, in high momentum transfer processes the dynamical content of these contact interactions are increasingly important and the current review addresses the recent progress in these studies. From the nuclear physics point of view this is the region dominated by short range multi-nucleon correlations. The understanding of the dynamics of these correlations has important relevance not only to the QCD dynamics of nuclear forces but also to the physics of high density nuclear matter that one expects to exist at the cores of neutron stars.

Importance of Short-Range Correlations: The atomic nucleus, as a bound system of interacting fermions with the Hamiltonian not commuting with the momentum operator, creates the phenomenon of momentum distribution of its constituents in the nucleus. Fermi statistics, combined with the fact that the combined volume of A nucleons is comparable to the nuclear volume, makes the effect of the nucleon correlations a phenomenon that ranges from the long to short distances. Long range correlations are reasonably well studied experimentally and have been understood based on Pauli blocking effects and the long-range part of the nuclear forces (2). Short-range nucleon correlations, on the other hand, represent the most intriguing part of the nuclear dynamics whose experimental studies are intensifying with the emergence of high energy accelerators capable of performing nuclear experiments with high intensity beams, allowing for precision measurements of small cross-sections.

Historically, the importance of short range correlations (SRCs) was first emphasized by R. Jastrow (3) who observed that application of variational methods to estimate the upper limit of the ground state energy fails for the problem involving strong interaction whose range, r_0 , is comparable with the size of the nucleons. In this case, the expectation value of the mean potential energy per nucleon is: $\bar{V} = \frac{Nr_0^3}{\Omega} |V_0|$, with Ω being the nuclear volume and V_0 the average potential of the NN interaction at $r \leq r_0$. From this relation one observes that in the hard sphere limit of the NN interaction core, the upper bound of the ground state energy increases without limit. This problem was solved (3)

by introducing NN correlations at $r \leq r_0$ distances based on the cluster decomposition approach choosing an ad-hoc form for the correlation function. While this approach solved the ground state energy problem it did not address the dynamical origin of such correlations. About the same time the correlation functions were introduced within the framework of the Brueckner - Goldstone theory (for the review and relevant references see Ref.(4)), in which the nucleon's finite size introduced a positional correlations that modified the independent particle state wave function.

An approach which demonstrated how the dynamical property of strong forces at short distances enters into SRCs was illustrated in Ref. (5) by obtaining the asymptotic solution of the N-body Schroedinger equation in the large momentum limit of the bound nucleons. In this case for specific behavior of the NN potential at short distances (see below) the momentum distribution of high momentum nucleon is defined as $n(p) \sim \frac{|V(p)|^2}{p^4}$. This relation indicates that probing large momentum of the bound nucleon in the nucleus allows to access the NN potential at large relative momenta or small relative distances. It is worth mentioning that the observation of the relation between short distance phenomena in the nucleus and high momentum component of nuclear wave function was already made within Brueckner-Goldston theory (see e.g. Ref.(6)) however the analytic property of NN potential was not identified for which the high momentum component would have the above presented form.

This approach defines the *main strategy* of SRC studies, which is, accessing the dynamics of NN interactions at short distances by probing bound nucleons with large initial momentum and removal energy.

Another issue that SRC studies aim to address is the existence of 3N and possibly higher order correlations. The questions in this case are whether SRCs of more than two nucleons can be formed and the necessary conditions to generate deeply bound high-momentum nucleons. These studies have significant astrophysical importance in understanding the dynamics of the super-dense nuclear matter which is formed in the core of the neutron stars.

Finally, a new direction of SRC studies is to probe the QCD content of these high density fluctuations. Recent experiments have begun to probe quark distributions in the kinematic region in which single quark carries momentum larger than the individual nucleon and are referred to as super-fast quarks.

Experiments with High Energy and High Intensity Beams:As introduced above, the main experimental methodology of accessing SRCs is to probe a deeply bound nucleon in the nucleus with large momentum and removal energy. To realize such a possibility one needs processes in which the energy transferred to the nucleon in the SRC significantly exceeds the potential and kinetic energies characteristic of the SRC. Such an instantaneous removal of the deeply bound nucleon from the SRC will release correlated nucleons, the detection of which will provide an additional window into the dynamics of SRCs in the nucleus.

Such experiments are only possible with high energy probes. The first possibility presented itself at Stanford Linear Accelerator Center (SLAC) where electron beams with up to 20 GeV energy made it possible to perform unprecedented measurements of inclusive $A(e, e')X$ processes in the kinematic region dominated by SRCs (7, 8, 9, 10, 11). These experiments allowed, for the first time, to reach the high-momentum component of nuclear wave function through the y -scaling analysis(12). Subsequently, the study at Jefferson Lab (13) of

the ratios of inclusive cross sections of nuclei A to the deuteron revealed the first signatures of two-nucleon SRCs in the form of the scaling as a function of Bjorken variable x in the region of $1 < x < 2$.

Meanwhile, attempts were made to extend the SRC studies to semi-inclusive processes in which the knock-out proton or the proton emerging from the 2N SRCs as a spectator, were detected in the coincidence with the scattered electron (13, 14, 15, 16). These experiments observed unambiguously the SRC signatures in the form of correlations between missing energy and missing momentum (14) or through the shifts of the scattered electron spectra proportional to the energy and angle of spectator protons (15, 16). However, such signatures are present for any two-body currents and due to restricted magnitudes of transferred energy and momentum it was impossible to dynamically suppress the soft two-body processes not related to SRCs (such as meson exchange currents).

The situation was completely changed with the emergence of CEBAF's 6 GeV continuous electron beam at Jefferson Lab (JLab), where practically all the major advances in SRC studies have been made in recent years. JLab's high energies along with high intensities of the electron beam allowed precision measurements of small cross-sections characteristic of SRC dynamics in electroproduction reactions. Additionally, triple coincidence experiments were carried out where additional nucleons were detected: one struck from the SRC by a virtual photon and the other emerged as a spectator from the same SRC. It is worth mentioning that about the time when JLab experiments were producing first results, SRC studies were also performed at Brookhaven National Laboratory (BNL). In the BNL experiments the AGS was used as a source for the high energy proton beams (6-15 GeV/c) to perform double $A(p, 2p)X$ and triple $A(p, 2pn)X$ coincident experiments aimed at SRC studies. Measurements of both electro-nuclear and proton-nuclear experiments were remarkable as they yielded almost identical results on the dynamics of SRCs, thereby confirming the universal nature of the object they were probing in the nucleus.

These experiments further stimulated the theoretical research on SRCs, covering issues related to high energy electro-nucleon processes, modeling high-momentum components of nuclear wave function, understanding the dominance of proton-neutron component in the SRCs and understanding of the role of the SRCs in medium modification of the bound nucleons. These together with the recent results in experimental studies of SRCs are the subject of the current review.

Summary of the Recent Progress: The series of recent experiments studying high energy eA and pA processes (17, 18, 19, 20, 21, 22, 23) have greatly improved our understanding of the dynamics of 2N SRCs in nuclei. The new generation of inclusive $A(e, e')X$ experiments (17, 18, 19) confirmed the observation made from the analysis of SLAC data (24, 25) that the ratios of nuclear to deuteron cross sections scale in the kinematic region dominated by the scattering from the 2N SRC. The ratios, designated by the parameter, $a_2(A, Z)$, directly related to the SRC strength in the high-momentum component of nuclear wave functions were measured for a wide range of A .

Analysis of the $A(e, e')X$ data in the deep-inelastic region at Jefferson Lab yielded EMC ratios which characterize the extent of medium modification of partonic distributions of the bound nucleon (26). Comparison of the strengths of the EMC ratios with the $a_2(A, Z)$ parameters revealed an apparent correlation between these two observables (27, 28), strongly suggesting that the medium modification effect is related to the probability of nucleons being in short-range correlations.

The final group of SRC experiments consisted of high-energy, semi-inclusive triple-

coincidence measurements (20, 22), which succeeded in probing the isospin composition of 2N SRCs in the relative momentum range of $\sim 250 - 650$ MeV/c. These experiments observed a strong (by factor of 20) dominance of the proton-neutron SRCs in nuclei as compared to the proton-proton and neutron-neutron correlations. Such an excess is understood (20, 29, 30) based on the dominance of the tensor forces in the NN interaction at the above mentioned momentum range corresponding to the average inter-nucleon separations of ~ 1.1 fm.

Based on the observation of the strong dominance of pn SRCs, it was predicted in Ref. (31, 32) that single proton or neutron momentum distributions in the 2N SRC domain are inversely proportional to their relative fractions in nuclei. This prediction is in agreement with the results of variational Monte-Carlo calculation of momentum distributions of light nuclei (33) as well with the SRC model calculation for medium to heavy nuclei (34). The recent experimental verification of the pn dominance in heavy nuclei (up to ^{208}Pb) (23) provides strong evidence for the universality of the above prediction across nuclei.

The isosinglet pn dominance in the SRC region makes the dedicated studies of the high-momentum component of the deuteron wave function a priority. The first experiment aimed at probing deuteron at large internal momenta was completed recently at JLab (35). Here, the exclusive $d(e, e'p)n$ cross section was measured at unprecedentedly large $Q^2 = 3.5$ GeV². This experiment succeeded for the first time in measuring deuteron momentum distribution for up to 550 MeV/c with negligible and controlled effects due to long-range nuclear phenomena and final state interactions. This experiment will be extended to even more extreme kinematics with the upgraded 12 GeV JLab accelerator. The experimental progress summarized above has stimulated strong theoretical activity in understanding the dynamical origin of short-range correlations and their implications in the different nuclear phenomena, including the EMC effect, symmetry energy and the nuclear contact (36, 37, 38, 39, 40, 41, 42, 43, 44, 45).

2. Recent Advances in Theory

2.1. Emergence of Short Range Correlations in Strongly Interacting Fermi Systems

While in Jastrow's paper (3) the correlation picture of multi-nucleon system was discussed within cluster development approach, it did not address the dynamical origin of the correlations. Such a discussion first was made in Ref.(5) where it was shown that in the limit of very large internal momenta of the bound nucleon, the solution of the Lipman-Schwinger equation is defined at large relative momentum of the pair-wise NN interaction potential. However, this work did not discuss whether the two-nucleon correlations will dominate the large momentum component of the nuclear wave function relative to the higher order (more than two nucleon) correlations. Subsequent works (46) analyzed the issue of hierarchy of NN correlations and observed that if the NN potential is a finite-range potential and in the high-momentum ($q \gg m_N$) limit behaves as $V(q) \sim \frac{1}{q^n}$ (with $n > 1$), then the wave function of the multinucleon system in the limit where one of the nucleons has a large momentum, is dominated mainly by two-nucleon correlations.

One can see such an emergence of 2N SRCs considering the Lipmann-Schwinger equation for a A-nucleon bound system interacting through the finite-range pair-wise NN interac-

tions, $V_{i,j}$, in the form

$$\phi_A(k_1, \dots, k_n, \dots, k_A) = \frac{-\frac{1}{2} \sum_{i \neq j} V_{ij}(q) \phi_A(k_1, \dots, k_i + q, \dots, k_j - q, \dots, k_A) \frac{d^3 q}{(2\pi)^3}}{\sum_{i=1}^A \frac{k_i^2}{2m_N} - E_B}, \quad (1)$$

where this equation can be used in the iteration approach to calculate the full nuclear wave function. If one starts with the first iteration using the mean-field nuclear wave function in the RHS part of the equation and considers one of the bound nucleons (say j) in the LHS part having momentum p such that $\frac{p^2}{2m_N} \gg E_B$, one observes that the integral in the RHS part will be dominated by the configuration in which $\mathbf{q} \approx \mathbf{p}$ such that $\mathbf{k}_j - \mathbf{q} \approx \mathbf{0}$ and $\mathbf{k}_i \approx -\mathbf{k}_j \approx -\mathbf{p}$ such that $k_i + q \approx 0$. This situation results in a two-nucleon correlation with large relative momentum such that (5):

$$\phi_A^{(1)}(k_1, \dots, k_i = p, \dots, k_j \approx -p, \dots, k_A) \sim \frac{V_{NN}(p)}{p^2} f(k_1, \dots, \dots, k_A), \quad (2)$$

where $f(\dots)$ is a smooth function of the momenta of non-correlated nucleons not containing momenta k_i and k_j . However this result does not yet guarantee the dominance of 2N correlations in the high momentum part of the nuclear wave function. In order for this to happen, higher order correlations should be parametrically small. In the approximation of pair-wise interaction the higher order correlations correspond to the higher order iterations. For example, 3N SRCs can be estimated by inserting Eq.(2) into Eq.(1), yielding:

$$\phi_A^{(2)}(\dots p, \dots) \sim \frac{1}{p^2} \int \frac{V_{NN}(q)V_{NN}(p)}{(p-q)^2} d^3 q. \quad (3)$$

If now one assumes analytic behavior for the NN potential of the form $V_{NN}(q) \sim q^{-n}$ in the large q limit, then one estimates the parametric dependence of the wave function due to three nucleon SRCs as:

$$\phi_A^{(2)}(\dots p, \dots) \sim \frac{V(p)}{p^2} \int_{q_{min}}^{\infty} \frac{dq}{q^n}, \quad (4)$$

where q_{min} is due to finite range of the potential. This relation indicates that for the finite-range interaction with $n > 1$, the second (as well as higher order) correlations will be parametrically suppressed (see also Refs. (25, 20)).

An important feature of the above result is that one will also arrive at the same conclusion in the relativistic framework if the nuclear dynamics are described within light-front or Weinberg-type equations for the bound systems (see e.g. (47, 46)).

The above discussion allows us to conclude that bound systems interacting through the pair-wise Yukawa type interactions will generate correlations dominated by two nucleon NN SRCs. Higher order correlations are possible but they are parametrically suppressed relative to 2N SRCs.

To access such correlations experimentally, one needs to probe bound nucleons with high initial momenta, requiring $\frac{p^2}{2m_N} \gg E_B$. If such conditions are met, then the asymptotic form of Eq.(2) leads to the following approximate relation for a nucleon momentum distribution at $p > k_F$, with k_F being the characteristic Fermi momentum of the nucleus:

$$n^A(p) \sim a_{NN}(A) \cdot n_{NN}(p), \quad (5)$$

where the full momentum distribution is normalized as $\int n^A(p)d^3p = 1$. The parameter $a_{NN}(A)$ can be interpreted as a probability of finding NN SRC in the given nucleus A . The function, $n_{NN}(p)$ is the momentum distribution in the NN SRC.

2.2. Conceptual Issues in High Energy Nuclear Theory

2.2.1. Emergence of Light-Front Dynamics. The above discussion indicates that probing short distance correlation structure of the nucleus requires probing a bound nucleon with momentum significantly exceeding the characteristic Fermi momentum, $k_F \sim 250 \text{ MeV}/c$. To achieve an instantaneous removal of such a nucleon from the nucleus, the momentum, q , transferred to the bound nucleon should be sufficiently large: $q \gg 2k_F$. Another restriction to the momentum transfer follows from the dynamic picture of SRCs, in which the correlated nucleons have large and comparable momenta in opposite directions. Therefore, in order to unambiguously discriminate the struck nucleon in the final state with momentum $\mathbf{p}_f = \mathbf{p}_i + \mathbf{q}$ from the correlated spectator nucleon (p_s), one needs to satisfy the condition of:

$$q \sim p_f \gg p_s \sim 300 - 1000 \text{ MeV}/c \quad (6)$$

Requiring that the interaction off the bound nucleon is quasi-elastic allows us to determine \mathbf{p}_i and leads to the kinematic threshold of $Q^2 = \mathbf{q}^2 - q_0^2 > m_N^2$. Thus one arrives at the optimal kinematics for probing SRC structure of nuclei as:

$$Q^2 > m_N^2, \quad q \sim p_f \geq \text{few GeV}/c, \quad p_s \sim \text{few hundred MeV}/c \quad (7)$$

These kinematic conditions bring us to the domain of high energy physics, meaning that the constituent masses of the bound system become increasingly less important. From the theoretical point of view, such a condition indicates an increased validity of the methods of high energy physics (48) associated with the onset of the light-front dynamics and calculational methods utilizing a new kind of (kinematic) small parameter such as

$$\frac{q_-}{q_+} \sim \frac{p_{f-}}{p_{f+}} \ll 1, \quad (8)$$

where $q_{\pm} = q_0 \pm \mathbf{q}$ and $p_{f\pm} = E_f \pm p_f^z$, with z -axis defined to be the direction of \mathbf{q} . Such a small parameter allows for systematic accounting of the strong off-shell effects in the reaction mechanism of the external probe - bound nucleon scattering (49) as well as the possibility for self-consistent calculation of the final state interaction of the fast struck nucleon with the correlated spectators within generalized eikonal approximation (50, 49, 51).

The emergence of light-front dynamics in which the scattering process evolves along the light-cone, $t \sim z$, is similar to that of deep-inelastic scattering (DIS) from a nucleon in which the parton distribution of nucleons is probed. Light-front dynamics in DIS is the most natural approach, since due to the light masses of quarks one deals with a large contribution from vacuum fluctuations which can be suppressed in the light-front or infinite momentum reference frames (see e.g. Refs. (48, 52)).

Vacuum fluctuations arise also in relation to the high momentum component of the nuclear wave function. With the momentum of the nucleon, p_i , becoming comparable with nucleon masses ($p_i \sim m_N$) the vacuum diagrams representing $N\bar{N}$ fluctuations become as important as diagrams representing the "valence" component of nuclear wave function (see e.g. Refs. (46, 53)). This is an important problem which should be addressed in

any theoretical studies aimed at the exploration of the high-momentum component of the nuclear wave function.

Another implication of light-front dynamics is the emergence of the light-cone variables (α_i, p_T) describing different nuclear "observables"¹ such as the nuclear spectral or light-front density functions. The variable, α_i , is analogous to the variable x of QCD and represents the light cone nuclear momentum fraction carried by the constituent nucleon and defined as

$$\alpha_i = \frac{p_{i-}}{p_{A-}/A}, \quad (9)$$

where p_{i-} and p_{A-} are "longitudinal" components of the light-cone momenta of the bound nucleon and nucleus².

One of the advantages of (α_i, p_T) variables is invariance with respect to Lorentz boosts in the \mathbf{q} direction. Such a feature allows to formulate nuclear spectral and density functions in a boost invariant form. These functions are nucleonic analogues of unintegrated partonic distribution functions in QCD and can be systematically extracted from the analysis of nuclear processes. However, the extraction is only possible provided the validity of factorization between the reaction mechanism and nuclear light-front momentum distributions as well as closure approximation for the final state interaction contribution. All these factors are analogous to DIS processes and can be systematically taken into account in the orders of the small parameter presented in Eq.(8) (see e.g. Ref.(49)).

If the light-front spectral or density functions are extracted, they will represent a testing ground for the light-front nuclear wave function, $\psi_A(\alpha_1, p_{T1}, \alpha_2, p_{T2}, \dots \alpha_A, p_{TA})$, through which the nuclear spectral and the density functions are constructed as follows:

$$P_A^N(\alpha_i, p_{Ti}, \tilde{M}_N^2) = \sum_{j=1}^A \int | \psi_A(\alpha_1, p_{T1}, \alpha_2, p_{T2}, \dots \alpha_A, p_{TA}) |^2 \delta(\alpha_i - \alpha_j) \delta^2(p_{Ti} - p_{Tj}) \times \delta(\tilde{M}_N^2 - (p_A - \sum_{j \neq i=1}^A p_j)^2) \prod_j \frac{d\alpha_j}{\alpha} d^2 p_{Tj} \quad (10)$$

and

$$\rho_A^N(\alpha, p_T) = \int P_A^N(\alpha_i, p_{Ti}, \tilde{M}_N^2) \frac{1}{2} d\tilde{M}_N^2 \quad (11)$$

normalized to the baryonic number of the nucleus:

$$\sum_N^A \int \rho_A^N(\alpha, p_T) \frac{d\alpha}{\alpha} d^2 p_T = A. \quad (12)$$

It is worth noting that ρ_A^N can be related to $f_A(\alpha, p_T)$ which is analogous to the unintegrated partonic distribution function in QCD, via:

$$f_A(\alpha, p_T) = \frac{\rho_A^N(\alpha, p_T)}{\alpha} \quad (13)$$

¹They are not direct observables, but ones that can be extracted from different scattering processes involving nuclear targets.

²Note that in our definitions the direction of the z axis is defined by the direction of the momentum transfer q , which is opposite to that of frequently defined in QCD analysis of the nucleon wave function (see e.g. (52)).

These functions, extracted from the high-momentum transfer semi-inclusive and inclusive processes, can provide a testing ground for the SRC properties of the nuclear wave function.

2.3. Nuclear Dynamics at Sub-Fermi Distances - pn Dominance

Emergence of NN correlations in the short-range nuclear dynamics creates a possibility of observing a host of new phenomena related to the rich structure of nucleon-nucleon interaction at short distances. One such effect arises from the interplay of the central and tensor parts of the NN potential, in which due to the repulsive core, the central part of the potential changes its sign at ~ 1 fm to become repulsive while no such transition exists for the tensor part of the potential. As a result, at NN separations of $r_{NN} \sim 1 \pm 0.2$ fm there is a clear dominance of the tensor part of the NN interaction compared to the central potential.

This situation creates an interesting selection rule for the isospin composition of the SRCs. The tensor operator does not couple to isotriplet states, i.e. $\hat{S}_{NN} | NN^{I=1} \rangle = 0$, resulting in a situation where the NN SRC is dominated by the isosinglet component of the pn pair.

If the contribution of pp , nn and isotriplet pn SRCs are negligible, one expects that in the momentum region of $\sim k_F - 600$ MeV/c the momentum distribution in the NN SRC is defined by the isosinglet pn correlation only. Using this fact and the local nature of SRCs one predicts:

$$n_{NN}(p) \approx n_{pn}(p) \approx n_d(p), \quad (14)$$

for Eq.(5), where $n_d(p)$ is the deuteron momentum distribution at $\sim k_F < p \leq 600$ MeV/c.

2.3.1. Two New Properties of High Momentum Component of Nuclear Wave Function.

We introduce the individual momentum distributions of proton ($n_p^A(p)$) and neutron ($n_n^A(p)$) such that:

$$n^A(p) = \frac{Z}{A} n_p^A(p) + \frac{A-Z}{A} n_n^A(p), \quad (15)$$

and $\int n_{p/n}^A(p) d^3p = 1$. Here, the terms in the sum represent the probability density of finding a proton or neutron with momentum p in the nucleus.

I. Approximate Scaling Relation: Integrating Eq.(15) within the momentum range of $\sim k_F - 600$ MeV/c one observes that the terms in the sum give the total probabilities of finding a proton and a neutron in the NN SRC. Since the SRCs, within the approximation where the contributions from the isotriplet NNs are negligible, consist only of the isosinglet pn -pairs, the total probabilities of finding proton and neutron in the SRC are equal. With the other possibilities for the SRC composition neglected, one predicts that in $\sim k_F - 600$ MeV/c region:

$$x_p \cdot n_p^A(p) \approx x_n \cdot n_n^A(p), \quad (16)$$

where $x_p = \frac{Z}{A}$, $x_n = \frac{A-Z}{A}$. This represents the *first property*, according to which the momentum distributions of proton and neutron weighted by their respective fractions are approximately equal.

The validity of the above approximate scaling rule is presented in Fig.1 where Eq.(16) is checked for the ${}^3\text{He}$ nucleus using the solution of Faddeev's equation (54), and for ${}^{10}\text{Be}$ using the results of variational Monte Carlo (VMC) calculations of Ref.(33). The solid lines

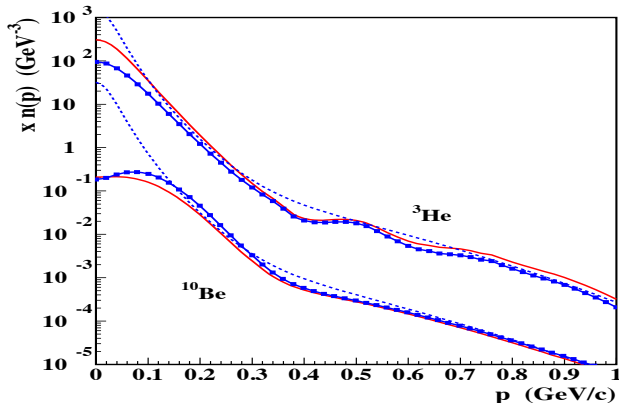


Figure 1: (color online) (a) The momentum distributions of proton and neutron weighted by x_p and x_n respectively. The dotted lines represent the prediction for the momentum distribution according to Eq.(17). (b) The $x_{p/n}$ weighted ratio of neutron to proton momentum distributions. See the text for details. Figure adapted from Ref.(31).

with and without squares in Fig.1 represent neutron and proton momentum distributions for both nuclei weighted by their respective x_n and x_p factors.

As can be seen in the figure, for ${}^3\text{He}$, the proton momentum distribution dominates the neutron momentum distribution at small momenta just because there are twice as much protons in ${}^3\text{He}$ and no specific selection rules exist for the mean field momentum distributions. The same is true for ${}^{10}\text{Be}$ for which now the neutron momentum distribution dominates at small momenta. However at ~ 300 MeV/c for both nuclei, the proton and neutron momentum distributions become close to each other up to the internal momenta of 600MeV/c. This is the region dominated by tensor interaction. Note that the similar features present for all other asymmetric nuclei calculated within the VMC method in Ref.(33) for up to $A \leq 11$.

II. Fractional Dependence of High Momentum Components: Using relations (5) and (14) for the high momentum distribution $n^A(p)$ and relation (16) from Eq.(15) one obtains that in $\sim k_F - 600$ MeV/c range

$$n_{p/n}^A(p) \approx \frac{1}{2x_{p/n}} a_2(A, y) \cdot n_d(p), \quad (17)$$

where $a_{NN}(A) \approx a_{pn}(A, y) \equiv a_2(A, y)$ and the nuclear asymmetry parameter is defined as $y = |x_n - x_p|$.

According to Ref.(31), for the situation in which the asymmetry parameter can be considered small, ($y < 1$), the NN correlation factor $a_2(A, y) \approx a_2(A, 0)$ which is a slowly changing function of nuclear mass for $A > 4$. This allows us to formulate the *second* property of the high-momentum distribution of nucleons: that, according to Eq.(17), *the probability of a proton or neutron being in high-momentum NN correlation is inversely proportional to their relative fractions (x_p or x_n) in the nucleus.*

We check the validity of this relation by comparing the momentum distribution in the NN SRC domain based on Eq.(17) with the realistic distributions presented in Fig.1. For this

Table 1: Fractions of high momentum protons and neutrons in nuclei A.

A	$P_p(\%)$	$P_n(\%)$	A	$P_p(\%)$	$P_n(\%)$
12	20	20	56	27	23
27	24	22	197	31	20

we use the estimates of a_2 for ${}^3\text{He}$ and ${}^{10}\text{Be}$ from Refs. (32, 19) and the deuteron momentum distribution n_d calculated using Argonne V18 NN potential (55), which were also used to calculate the realistic momentum distributions for ${}^3\text{He}$ and ${}^{10}\text{Be}$. As can be seen from these comparisons, Eq.(17) works rather well starting at 200 MeV/c and surprisingly for up to the momenta ~ 1 GeV/c, indicating that the 3N SRCs are parametrically small for all momenta (as discussed in Sec.2.1).

2.3.2. Momentum Sharing in Asymmetric Nuclei. The important implication of the *second property* is that the relative number of high momentum protons and neutrons becomes increasingly *unbalanced* with an increase of the nuclear asymmetry, y . To quantify this prediction, using Eq.(17) one calculates the fraction of the nucleons having momenta $\geq k_F$ as:

$$P_{p/n}(A, y) \approx \frac{1}{2x_{p/n}} a_2(A, y) \int_{k_F}^{\infty} n_d(p) d^3p, \quad (18)$$

where we extend the upper limit of integration to infinity because of the smaller overall contribution from the ≥ 600 MeV/c region. The results of the calculation of $P_{p/n}$ s for medium to heavy nuclei, using the estimates of $a_2(A, y)$ from Ref. (24, 17, 18, 32, 19) and k_F from Ref. (56) are given in Table.1.

The estimates in Table.1 indicate that with the increase of asymmetry y , the imbalance between the high-momentum fractions of proton and neutron grows. For gold, the fraction of high-momentum protons exceeds that of the neutrons by as much as 50%.

Table 2: Kinetic energies (in MeV) of protons and neutrons across several nuclei

A	y	E_{kin}^p	E_{kin}^n	$E_{kin}^p - E_{kin}^n$
${}^8\text{He}$	0.50	30.13	18.60	11.53
${}^6\text{He}$	0.33	27.66	19.06	8.60
${}^9\text{Li}$	0.33	31.39	24.91	6.48
${}^3\text{He}$	0.33	14.71	19.35	-4.64
${}^3\text{H}$	0.33	19.61	14.96	4.65
${}^8\text{Li}$	0.25	28.95	23.98	4.97
${}^{10}\text{Be}$	0.2	30.20	25.95	4.25
${}^7\text{Li}$	0.14	26.88	24.54	2.34
${}^9\text{Be}$	0.11	29.82	27.09	2.73
${}^{11}\text{B}$	0.09	33.40	31.75	1.65

Another implication of Eq.(18) is that due to the larger relative fraction of high momentum the minority component should be more energetic in asymmetric nuclei than the majority component. Namely, one expects a more energetic neutron than proton in ${}^3\text{He}$ and the opposite result for neutron rich nuclei. This expectation is confirmed by ab-initio calculation of p - and n - kinetic energies for all nuclei (currently up to $A \leq 11$) (see Table 2 and Ref. (31) for more details).

2.4. Three Nucleon Correlations

In the previous discussion, we defined a nucleon to be in a 2N SRC if its momentum exceeds k_F and almost entirely compensated by the momentum of the correlated nucleon in the nucleus. For a nucleon to be in a 3N SRC we assume, again, that its momentum significantly exceeds k_F but in this case is balanced by two correlated nucleons with momenta $> k_F$. In both cases the center of mass momentum of the SRC, $p_{cm} \leq k_F$.

In principle, the complete nuclear wave function should contain the above-described property of 2N and 3N SRCs. Unfortunately, the calculation of such wave functions from first principles is currently impossible due to poorly understood strong interaction dynamics at short nuclear distances as well as relativistic effects that become increasingly important at large momenta of nucleons involved in short range correlations. However, recent theoretical studies have provided a sufficient roadmap for meaningful experimental exploration of 3N SRCs.

One result of such studies is that the irreducible three-nucleon forces contribute to 3N SRCs only at very large nuclear excitation energies of $> 2(\sqrt{p^2 + m_N^2} - m_N)$, $p \gtrsim 700$ MeV/c, and are otherwise negligible (29). Thus, outside of such kinematic regions, the dynamics of 3N SRCs are defined by two successive short-range NN interactions (57). Such a situation highlights the difficulties of experimental identification of 3N SRCs. From the point of view of extracting the nuclear spectral function, the separation of 3N SRCs are problematic since the expected enhancement in recoil energy distribution at $E_{rec} \approx p^2/4m_N$ is very broad without a discernible maximum (29). With regard to the momentum distribution, as the 3N SRCs are subleading compared to 2N SRCs (58) (see also Sec.2.1), they are parametrically small for all p making the momentum distribution $n_A(p)$ rather insensitive to 3N SRCs.

Hence, one of the problems in experimental identification of 3N SRCs is a proper identification of the variables that can unambiguously discriminate 3N and 2N SRCs. To this end, the relevant variable is the light-cone momentum fraction, α_i defined in Eq.(9). Due to the short-range nature of nuclear forces the condition

$$j - 1 < \alpha_i < j \quad (19)$$

will ensure that scattering from $(j \times N)$ -SRC is being probed (46, 58). Thus, one expects that the extraction of $\rho_A(\alpha_i)$ at $\alpha_i > 2$ will ensure the dominance of 3N SRCs.

Dynamics of the 3N SRCs: In light of the recent observation of strong dominance of pn pairs in 2N SRCs (Sec.2.3) for momenta of 250 – 600 MeV/c and the expectation (discussed above) that 3N SRCs are predominantly due to two successive 2N short-range interactions, one predicts a strong implication of the pn dominance in 3N SRCs as well. This means that 3N SRCs should predominantly have a ppn or nnp composition with ppp and nnn configurations being strongly suppressed. The diagram that will represent the light-cone density matrix of 3N SRCs is given in Fig.5(left panel), where three nucleons are either in ppn or nnp configuration. The light-front spectral function according to the diagram of Fig.5(left panel), calculated within effective Feynman diagrammatic approach (57, 59) is expressed through the light-front density functions of NN SRCs as follows:

$$P_{A,3N}^N(\alpha_1, p_{1,\perp}, \tilde{M}_N) = \int \frac{3 - \alpha_3}{2(2 - \alpha_3)^2} \rho_{NN}(\beta_3, p_{3\perp}) \rho_{NN}(\beta_1, \tilde{k}_{1\perp}) 2\delta(\alpha_1 + \alpha_2 + \alpha_3 - 3) \delta^2(p_{1\perp} + p_{2\perp} + p_{3\perp}) \delta(\tilde{M}_N^2 - M_N^{3N,2}) d\alpha_2 d^2 p_{2\perp} d\alpha_3 d^2 p_{3\perp}, \quad (20)$$

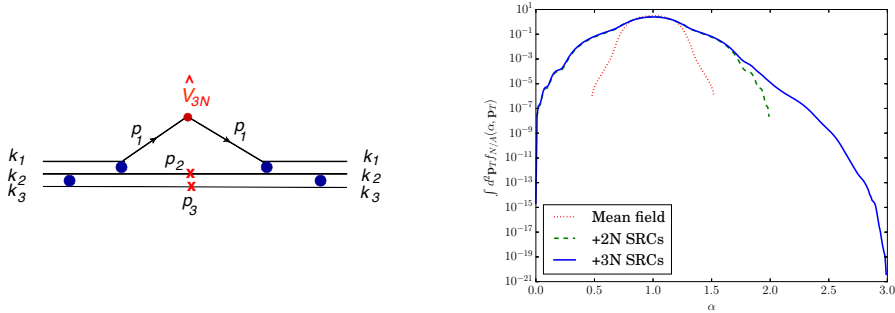


Figure 2: (left panel) The 3N SRCs due to sequential 2N short range correlations. (right panel) The α distribution of the light-front density matrix. Dotted - lines - nuclear mean field contribution only, dashed - mean-field and 2N SRC contribution, solid - mean field, 2N- and 3N SRCs included. Figure adapted from Ref.(59).

where within colinear approximation $\beta_3 = \alpha_3$, $\beta_1 = \frac{2\alpha_2}{3-\alpha_3}$ as well as $\tilde{k}_{1\perp} = p_{1\perp} + \frac{\beta_1}{2} p_{3\perp}$ with α_i representing the light-cone momentum fraction of 3N SRCs carried by the correlated nucleon i . The 3N SRC spectral function uses as an input the density functions of 2N SRCs, ρ_{NN} , which can be extracted from studies of two-nucleon correlations.

The dynamics of 3N SRCs, according to the correlation scenario of Fig.5(left panel), have several unique features that can be verified experimentally. One is that the per nucleon probability of finding a nucleon in a 3N SRC, a_{3N} , should be proportional to the square of the probabilities of 2N SRCs, a_{2N} , i.e.

$$a_{3N} \sim a_{2N}^2. \quad (21)$$

Another feature is that the dominant 3N SRC configuration will be one in which the two nucleon spectator system has a minimal mass $m_S \gtrsim 2m_N$, corresponding to small relative momentum in the recoil NN system, $k_{NN} = \frac{\sqrt{m_S^2 - 4m_N^2}}{2}$. The condition $k_{NN} \ll m_N$ and the fact that isotriplet two-nucleon states with low relative momenta are strongly suppressed (60) compared to the isosinglet states results in a strong dependence of the 3N SRCs on the isospin structure of NN recoil system. Namely, 3N SRCs are dominated by configurations in which the recoil two-nucleon system is in the isosinglet state.

We conclude the discussion on 3N SRCs illustrating a calculation of p_T integrated light-front density function (59) in Fig.5 (right panel) containing mean-field, 2N and 3N SRC contributions. As the figure shows, despite the 3N SRCs being subleading to the 2N SRCs, they are well separated in α , as was discussed above.

2.4.1. Non-Nucleonic Degrees of Freedom and Medium Modifications. Recent experimental and theoretical studies of SRCs have advanced our understanding of the domain of two-nucleon correlations for momenta up to 600 MeV/c. This provides important groundwork for the extension of SRC studies to the more uncharted territory of hadron-quark transition. The studies of isospin structure of NN SRCs (20, 21, 22) found not only the pn dominance but also observed that the sum of the absolute pp and pn probabilities are close to unity, indicating that practically all nucleons in this momentum range (with accuracy in the order of few%) belong to two nucleon SRC. This is an important observation since with

a high level of confidence it excludes the explicit non-nucleonic degrees of freedom in this momentum range.

By contrast, nucleons are composite particles, and therefore inter-nucleon interactions in SRCs should lead to a deformation of the bound nucleon wave function. Such a modification of the bound nucleon is manifested in the experimental observation of the difference between partonic distributions of the free and bound nucleons, commonly referred as EMC effect (61). The most recent EMC effect measurement was performed for the wide range of nuclear targets, focussing on light nuclei (26), with the interesting observation that the extent of the modification is not proportional to the average density of nuclei but rather to the local density at which the bound nucleon is probed. The last observation can possibly indicate the important role that SRCs play in the medium modification of the partonic distribution of nucleons in the nuclei. This expectation is further enhanced with the observation of apparent correlation between the strengths of the EMC effect and 2N SRCs (27, 28). Similar, apparent correlations (28) have been observed also between EMC effects and nuclear excitation energies all indicating the enhancing role of SRCs in the modification of the internal structure of bound nucleons.

2.5. Nuclear Dynamics at Core Distances

One of the most fascinating aspects of nuclear physics at short distances is the repulsive core. With the coming of age of high energy and high intensity accelerators such as CEBAF12, LHC and JPARC as well as currently discussed electron ion collider (EIC) there is a real possibility for systematic exploration of nuclear dynamics at core distances. We will characterize core distances as those where the probed relative distance is smaller than the radius of the nucleon which will mean substantial overlap of two nucleons in the nuclear medium.

Currently very little is known about the structure and the dynamics of nuclear repulsion at core distances. The modern NN potentials employ the Wood-Saxon ansatz while models based on one boson-exchanges introduce vector-meson exchanges to reproduce repulsion at distances smaller than the size of the exchanged mesons. QCD-based models employ other extreme scenarios in which two nucleons are collapsed into a six-quark state.

The relative momenta in the NN system which will be sensitive to the core dynamics can be estimated based on the threshold of inelastic $N \rightarrow \Delta$ transition:

$$\sqrt{M_N^2 + p^2} - M_N \geq M_\Delta - M_N \quad (22)$$

which results in $p \geq 800$ MeV/c. Thus one of the direct ways of reaching the core is to probe internal momenta in ~ 1 GeV/c region.

2.5.1. Super-Fast Quarks in Nuclear Medium. Experimentally, it is possible to probe internal momenta in nuclei in the range of ≥ 1 GeV/c by considering deep inelastic scattering from superfast quarks in nuclei (25, 62).

We define superfast quark as partons that have been probed via nuclear DIS scattering at Bjorken $x > 1$. Since in an isolated nucleon at rest partons cannot carry momentum fractions larger than one, DIS scattering at $x > 1$ is possible if partons in nearby nucleons are sharing momentum. This requires these two nucleons to be in very close proximity.

There are two basic reasons that superfast quarks probe high-density fluctuations in the nuclear medium. The first is kinematical. The initial longitudinal momentum of a nucleon

probed in DIS scattering is (62):

$$p_i^z = m(1 - x - x \left[\frac{W^2 - m^2}{Q^2} \right]), \quad (23)$$

where W is the final mass produced on the nucleon in the nucleus. As Fig.3(left panel) shows, in the DIS region at $W \geq 2.5$ GeV, the virtual photon will probe a nucleon with momentum $p_i^z \sim -1$ GeV/c.

The second reason that superfast quark probes very high-momentum component in the nuclear medium is dynamic. Due to QCD evolution, the parton at x is evolved from the original partons with momentum fractions $x_0 \geq x$ which increases with Q^2 . Thus, the alternative way of probing short space-time separations in the nuclear medium will be a measurement with fixed x and increasingly large Q^2 . Such studies will probe QCD dynamics in the extreme nuclear conditions with the potential of opening up uncharted territory for nuclear QCD.

The extreme nuclear dynamics may include multi-nucleon short range correlations (25, 62, 59), explicit quark degrees of freedom such as 6-quark clusters (63), or single-quark momentum exchanges between strongly correlated nucleons (64).

Superfast quarks can be probed in different processes including inclusive DIS from nuclei at $x > 1$ (25, 62, 64), the processes such as semi-inclusive nuclear DIS with tagged spectator nucleons (65, 66), DIS production in the forward direction with $x_F > 1$ or large transverse momentum dijet production in $p + A \rightarrow$ dijet + X reactions at LHC kinematics (59).

3. Recent Advances in Experiment

The beginning of Jefferson Lab's operation in 1990's started a truly new era in exploration of the nuclear structure at short distances. The SRC program included high Q^2 (≥ 1 GeV²) inclusive $A(e, e')X$ measurements(67, 68, 69, 17, 18, 19) complemented with semi-inclusive triple-coincidence(21, 22, 70, 23) and exclusive deuteron electrodisintegration(71, 35) experiments.

The most important results on NN SRCs have been obtained recently from inclusive and triple-coincidence measurements which we will review below.

3.1. Inclusive high Q^2 Processes at $x > 1$.

The main motivation in any experiment aimed at studying SRCs is to probe the bound nucleon with momentum exceeding characteristic Fermi momentum $k_F \sim 250$ MeV/c. As it was discussed in Sec.2.2, the more relevant quantity in this respect is light-front momentum fraction α_i (Eq.(9)) for which, choosing condition of Eq.(19) will allow to probe j -nucleon short range correlations. The technical question for a given experiment is how to determine the parameter α_i for different regions of NN correlation dominance.

One way to achieve such a measurement is in the quasilelastic nuclear reactions in which from the condition $(p_i + q)^2 = M_N^2$ one obtains:

$$\alpha_i = x \left(1 + \frac{2p_{i,z}}{q_0 + |q|} \right) + \frac{M_N^2 - m_i^2}{2m_N q_0}, \quad (24)$$

where $p_{i,z}$ is the longitudinal momentum of the initial nucleon along the direction of the transferred momentum q in the nuclear rest frame. From the above equation one observes

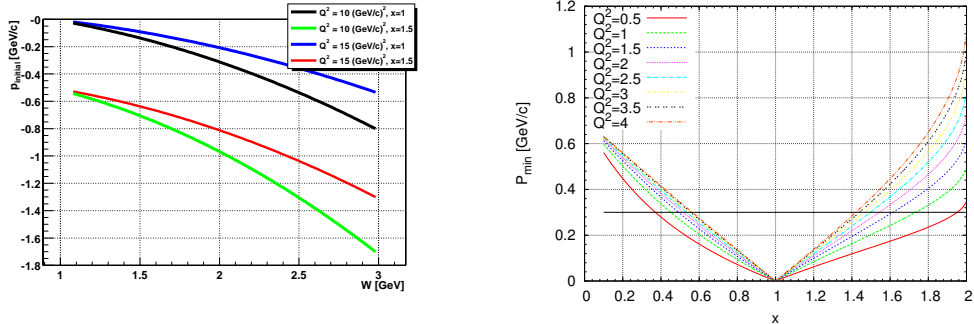


Figure 3: (left panel) Dependence of p_{in}^z on the final mass W produced in DIS scattering off the bound nucleon in the nucleus. (right panel) The minimum momentum for quasi-elastic $\gamma^* + 2N \rightarrow N + N$ scattering as a function of x for different values of Q^2 .

that in the asymptotic limit of large Q^2 , $\alpha_i \approx x$ and thus choosing $x > 1$ allows to satisfy conditions necessary to probe multi-nucleon correlations. Since Bjorken x is defined by kinematics of electron scattering only, $x = \frac{Q^2}{2M_N q_0}$, this consideration indicates that NN correlations can be probed in inclusive $A(e, e')X$ experiments.

3.1.1. Probing 2N SRCs in $1 < x < 2$ Region. In the above discussion we considered the asymptotically large Q^2 to illustrate the simple relation between α_i and Bjorken x . At finite values of Q^2 one can use Eq.(24) to identify the optimal kinematics for separation of 2N correlations. For this we notice that Eq.(24) can be solved for the longitudinal component of p_i that represents the minimal magnitude for the momentum of the bound nucleon. Then one can find the suitable x, Q^2 kinematics for which $|p_{min}| > k_{Fermi}$ to isolate 2N SRCs. Fig. 3(right panel) shows the relationship between p_{min} , x and Q^2 , leading one to conclude that to observe 2N SRCs at $x \geq 1.4$, a $Q^2 = 1.4$ GeV 2 is required. The figure also shows that one will not be able to probe correlations at $Q^2 \leq 1$ GeV 2 . The existence of such a threshold in Q^2 was experimentally observed in the dedicated measurement of inclusive cross sections at $x > 1$ in Refs.(17).

The minimal initial momentum of the bound nucleon can be used to estimate (24) the corresponding light-cone momentum fraction, α_{2N} which is defined by the parameters of scattered electron only:

$$\alpha_{2N} = 2 - \frac{q_- + 2m_N}{2m_N} \left(1 + \frac{\sqrt{W^2 - m_N^2}}{W^2} \right), \quad (25)$$

where $W^2 = 4m_N^2 + 4m_N \nu - Q^2$. The advantage of discussing the inclusive cross section based on α_{2N} representation is that in the high energy limit one expects that inclusive cross section to factorize into the product of cross section of electron-bound nucleon scattering and the light-front density matrix of the nucleus $\rho_A(\alpha_{2N})$. Therefore the inclusive scattering in principle allows an extraction of $\rho_A(\alpha_{2N})$ from the measured cross sections.

The first indication of the onset of 2N SRC regime in inclusive scattering is the appearance of the plateau in the ratios of the cross sections measured for nuclei A to the

deuteron(19) or ${}^3\text{He}$ (17, 18) in the $x > 1$ region at large Q^2 . This plateau is the result of the nuclear high momentum's factorization in the form of Eq.(17).

The recent results of such measurements are presented in Fig.4(left-hand side, plotted vs x) for ${}^3\text{He}/D$ and ${}^{12}\text{C}/D$ ratios. The different sets of colored points correspond to data taken at different Q^2 values, ranging from 2.5 GeV^2 to 7.4 GeV^2 (as evaluated at $x = 1$). Only points with uncertainties under 10% are shown, meaning that only the lowest Q^2 data reach the highest x values.

One of the interesting features of the x dependence of the experimental ratios is that the threshold for the onset of the scaling is pushed out further in x for ${}^{12}\text{C}$ as compared to the ${}^3\text{He}$. This can be understood from the fact that for heavier nuclei, k_{fermi} is higher, and the 2N SRC region begins at higher x values, as the mean-field contribution persists for longer.

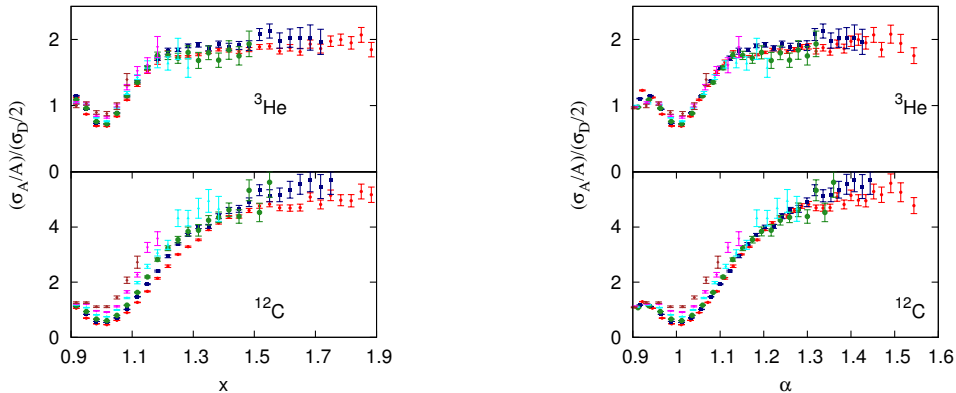


Figure 4: σ_A/σ_D vs x (left panel) and α (right panel) for selected targets from JLab E02-019 experiment. See text for details.

Another feature seen in the x dependence is that for given nucleus the onset of scaling is Q^2 -dependent. Such Q^2 dependence is more visible in the ${}^{12}\text{C}/D$ ratios where one observes that the data at higher Q^2 values rise towards the plateau value sooner. Such a Q^2 dependence can be understood from Eq.(25), where for a given x value, the α_{2N} values change with Q^2 . However if we consider the α_{2N} distribution of the ratios instead of x then such a Q^2 dependence should diminish. This is what is observed in the experimental data shown in the right-side panel of Fig. 4. This fact is one of the most important arguments for the validity of the 2N SRC picture of inclusive scattering.

Even though the observation of the plateau is consistent with the expectation of scattering from 2N SRCs, to study the dynamics of the SRCs in more detail, one needs to address several theoretical issues. One issue is the shape of the ratios. If the contribution in the $x > 1$ region is only from 2N SRCs, then the expectation is that the shape of the plateau, should be the same for both ${}^3\text{He}$ and ${}^{12}\text{C}$ and for other nuclear targets (19). The nuclear cross-sections can extend upto $x \approx A$, meaning the D cross-section has to go to zero by $x = 2$, whereas for $A > 2$, strength continues well past that. Therefore, we expect a slight rise in the A/D ratios as we approach the $x = 2$ limit. This rise due to different rates of cross-section fall-off between A and D gets larger with increasing nucleus size. Additionally,

for $A > 2$, the correlated pair will experience center-of-mass motion in the field of the other nucleons. This will distort the momentum distribution compared to that of the deuteron, enhancing the high-momentum tail region. Finally, $A > 2$ nuclei will have contributions from 3N correlations that could be appearing near the $x \approx 2$ region.

All of the above factors are essential for the extraction of the parameter $a_2(A, z)$ from the cross-section ratio. A correction is required for the center-of-mass motion of the pair, and a cut in α must be placed to isolate the region that is dominated by 2N correlations. The most recent analysis (19) did both, with a cut of $1.5 < \alpha < 1.9$ and rudimentary center-of-mass motion calculations, yielding corrections upto 20% for heavy nuclei. The calculation entails comparing a calculated deuteron momentum distribution to one smeared with realistic center-of-mass motion (72). Better evaluations of the center-of-mass corrections are desirable for future experiments.

3.1.2. Probing 3N SRCs in $x > 2$ Region. According to Eq.(19) accessing the region of $\alpha_i \geq 2$ will allow us to probe 3N SRCs. However, while in the case of the 2N SRCs one needs to simply go beyond k_F , for 3N SRCs, the transition from two- to three- nucleon SRCs is more complicated. Early measurements of inclusive cross-section ratios at $x > 1$ relied on the idea that a second plateau, corresponding to 3N strength should be observed at $2.4 \lesssim x \lesssim 3$ and $Q^2 \geq 1.4 \text{ GeV}^2$, analogous to the 2N SRC plateau in the $1.5 \lesssim x \lesssim 1.9$ region. Data from JLab’s Hall B that appeared to support this observation were first published by Ref. (18) with ${}^4\text{He}/{}^3\text{He}$, ${}^{12}\text{C}/{}^3\text{He}$, and ${}^{56}\text{Fe}/{}^3\text{He}$ ratios. However, a later experiment in JLab’s Hall C (19) did not observe a second plateau, albeit the uncertainties were significantly higher, thereby not excluding the possibility. The two sets of data showed excellent agreement in the 2N correlation region, as can be seen in Fig. 5. One possibility for this discrepancy was the different kinematics of the two measurements. As a kinematic threshold exists for the observation of 2N correlation plateaus, a 3N analog is expected, but the Q^2 threshold is not as easily obtained. The CLAS data were taken at an average Q^2 value of 1.4 GeV^2 compared to 2.7 GeV^2 for the Hall C data. Since 1.4 GeV^2 is the threshold for 2N correlations, one would expect needing a higher value to observe a 3N plateau, suggesting that the Q^2 of the CLAS data may have been too low. However, this does not explain away the apparent plateau at $x > 2.25$.

A recent reanalysis of the CLAS data (73) shows that this plateau can be the effect of bin migration. Both experiments measured cross sections as a function of the scattered energy of the electron (E') and converted to x . The resolution of the CLAS spectrometer is almost an order of magnitude lower than than of the High Momentum Spectrometer in Hall C, and at large x values, $x \geq 2$, it is larger than the size of the bins. This effect, combined with the fact that the ${}^3\text{He}$ cross-section is exponentially approaching zero in this region results in significant bin migration. Specifically, most of the points making up the 3N SRC plateau in the CLAS data (18) came from the same E' bin.

The question of why JLab E02-019, whose data were taken at higher values of Q^2 with a high resolution spectrometer, did not observe a 3N SRC plateau remains. In this respect one can consider the variable α_{3N} , a counterpart of α_{2N} for 2N SRCs in Eq.(25). Here, α_{3N} properly accounts for the mass of the 3N system and the recoil of the 2N system (assuming a configuration where one high-momentum nucleon is balanced by two others). From theoretical analysis of hadroproduction reaction, a minimum α value of 1.6 is required to isolate high-momentum nucleons born in 3N SRC. Fig. 5 (right hand side) shows that a minimum Q^2 of 5 GeV^2 is needed to access this region, whereas the existing JLab data

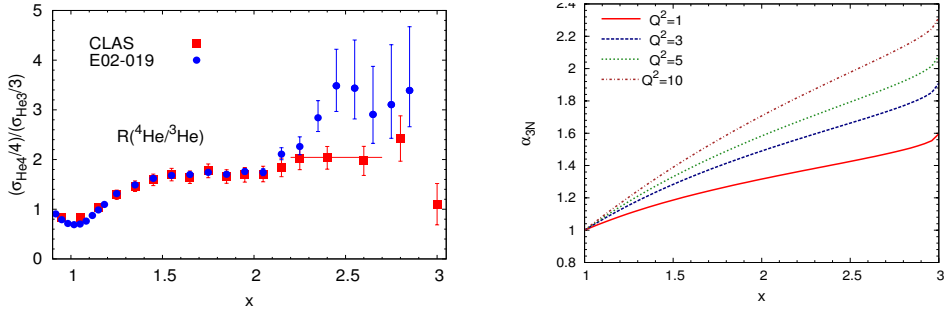


Figure 5: (left panel) The ratio of (e, e') cross section of ^4He and ^3He targets as a function of Bjorken x . Figure adapted from Ref.(19). (right panel) The α_{3N} relation to the Bjorken x for different Q^2 .

were taken below 3 GeV^2 . However $Q^2 \geq 5 \text{ GeV}^2$, is within reach at JLab with the 12 GeV upgrade. It also means that future analyses should be done using the $\alpha_{2n,3n}$ variables, rather than the traditional x , as they can unambiguously connect to 2N and 3N SRC dominance regions.

3.1.3. Upcoming Inclusive Measurements. JLab experiment E08-014 took data in Hall A with both of the High Resolution Spectrometers, focusing on the $x > 2$ region, aiming to map out the onset of the 3N plateau via a Q^2 scan as well as taking data with ^{40}Ca and ^{48}Ca targets to study the isospin dependence of SRC. Fig. 5 (right hand side) suggests that the kinematics probed by this experiment at 6 GeV were not sufficient to see a 3N plateau, but the precision of the data on the calcium target should be sufficient to yield interesting results.

JLab plans to perform additional inclusive SRC measurements are planned at JLab for the 12 GeV era. These include high-precision measurements on $A=3$ nuclei in Hall A that can be compared to calculations. Additionally, E12-06-105 will take data on a variety of nuclei, both light and heavy with scans in Q^2 to explore the onset of the 3N plateau as well as to study the nuclear dependence of 2N SRC. The most important aspects of SRC exploration with 12 GeV energy is the possibility of unambiguous verification of the existence of 3N SRCs, access to the domain of the nuclear repulsive core in the NN correlation as well as probing the superfast quarks in deep-inelastic inclusive processes at $x \lesssim 1$ kinematics (see Section 4.2).

3.2. Nucleon-Nucleon Correlations and the EMC Effect

In 1983 the European Muon Collaboration (EMC) published their surprise deep inelastic scattering result (61) which showed a dip in the per nucleon cross section ratio of heavy to light nuclei when plotted vs. Bjorken x : a ratio that naively one would expect to be unity up to the Fermi motion effects. This surprising result has been reproduced many times (74, 26, 75, 76) and this dip in the cross section ratio is now commonly referred to as the EMC effect. Many possible explanations for this unexpected phenomenological result

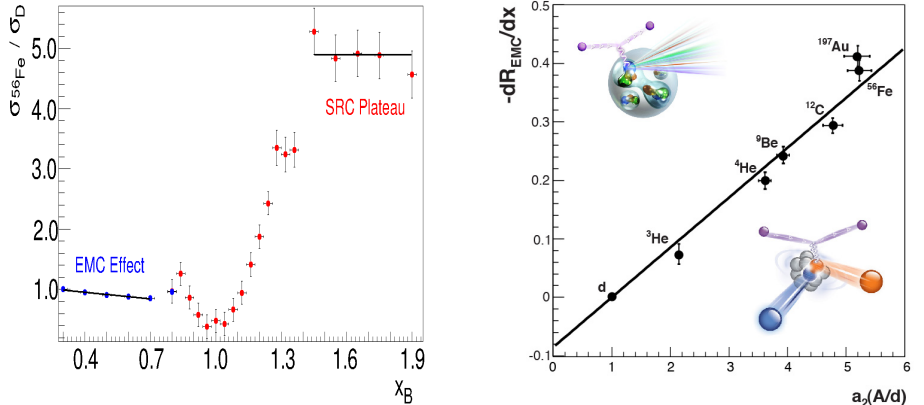


Figure 6: (*left panel*) The Bjorken x dependence of the ratio of inclusive (ee') cross section of ^{56}Fe to the deuteron targets. Figure adapted from Ref.(79). (*right panel*) Observed correlation between the strengths of the EMC effect and 2N SRCs. Figure used with permission from Jefferson Lab. Figure adapted from Ref.(80).

have been put forth over the years though no definitive solution to the EMC effect puzzle has been agreed upon. (77, 78, 79, 80).

In 2011, L. Weinstein *et al.* (27) noted a linear relation between the magnitude of the EMC effect and the magnitude of the aforementioned inclusive high-momentum plateaus as shown in Fig. 6. There is a clear linear relationship between these two seemingly disconnect phenomena which very well may be due to the short-range behaviors of the proton-neutron pairs in the nucleus (36). Later publications, which included more data, saw similar behaviors, though the data alone do not provide a clear cause for the relationship (28, 81).

A modern review on the topic of nucleon-nucleon correlations and the EMC effect points to the fact that the strongly interacting proton-neutron pairs which have been shown to be a universal aspect of high momentum nucleons in the nucleus may also be responsible for the modification of the structure functions. For a complete discussion of the possible connections between nucleon-nucleon correlations and quarks see the recent review by O. Hen *et al.* (36).

3.3. Recent ($e,e'p$) Measurements

Although nuclear theory long ago identified the need to include high-momentum components to nuclear momentum distributions and all modern nucleon-nucleon potentials generate high momentum tail in the nuclear wave function with a strength far beyond what one would expect from an independent particle models; it is nevertheless quite challenging to probe directly the high momentum component of the nuclear wave function. The above mentioned inclusive results as well as elastic nuclear scattering at large momentum transfers give a very strong indication of initial-state SRCs in the nuclear wave function allowing also to estimate their overall strength. However these processes did not allow to extract the shape of high momentum distribution allowing to probe only the integrated characteristics of SRCs. Thus a large experimental effort was put in place to measure knock-out ($e,e'p$) reactions to determine the shapes of high momentum distributions at large values of residual

nuclear excitation energies.

Early nucleon knock-out experiments, with $(e, e'p)$ missing momenta less than the Fermi momentum were successfully able to extract the momentum distribution of nucleon in the nucleus from the measured cross sections (82). It was also conjectured at the time, that by simply pushing to larger momentum transfer, it would be possible to extract the high momentum part of the momentum distribution; but here nature would not be so kind. As shown in many experiments, reaction mechanisms, final-state interactions or virtual nucleon excitations could quickly dominate the high momentum signal (83) making it extremely challenging to determine the initial-state high momentum distribution.

Part of the problem was the limited kinematics reach of the accelerators at the time. This limited the high missing momentum data to the region between the quasi-elastic peak and the delta resonance. A region commonly known as the "dip" region. With the advent of JLab, the first $(e, e'p)$ experiments have been measured at large missing momentum on the quasi-elastic peak ($x \approx 1$). The kinematics of these measurements corresponded to the large transverse component of missing momentum, resulting in a strong dominance of final-state interactions in the measured cross sections (84, 85, 86).

By pushing the kinematics to $Q^2 = 3.5 \text{ GeV}^2/c^2$ and making use of the previous result to minimize final state interaction effects it has been possible to isolate the high momentum component of the deuteron with minimum model dependence (35). Future $(e, e'p)$ experiments at Jefferson Lab with a 12 GeV beam will extend these kinematics even further, going to both large missing momentum, $Q^2 \gg 1$, and $x_B > 1$ (87). These kinematics will ideally satisfy the conditions of Eq.(7) allowing an access to the momentum distribution of the deuteron at unprecedentedly large values. Asymmetry measurements have also been useful in isolating SRC effects, though to date the unambiguous interpretation of the data require inclusion of several effects associated with long range two-body currents (88, 89, 90).

3.4. Triple Coincidence Processes

One of the most important recent advances in studies of the structure of SRCs has been made in triple coincidence experiments (20, 21, 22, 23). The possibility of reaching high enough momentum transfer that allows to distinguish between struck nucleon from the nucleon recoiled from the SRC allows to gain important information about the dynamics and the composition of SRCs.

3.4.1. Angular Correlation of Nucleons in the 2N SRC. The kinematics of these experiments were close to the one discussed in Eq.(7) in which the detected recoil nucleon with momentum p_r can be associated with the spectator nucleon.

From the theory point of view, such a reaction within PWIA will be described as:

$$\frac{d\sigma}{d\Omega_{e'} dE_{e'} d^3p_N dd^3p_r} = \frac{F_N}{F_A} \sigma_{eN} \cdot D_A(p_i, p_r, E_r), \quad (26)$$

where the decay function $D_A(p_i, p_r, E_r)$ (25, 29, 58), describes the probability that after a nucleon with momentum p_i is instantaneously removed from the nucleus, the residual $(A-1)$ nuclear system will have residual energy $E_R = q_0 - T_f$ and contain a nucleon in the nuclear decay products, with momentum p_r . Note that if factorization of the nucleon electromagnetic current is justified, then the decay function can be generalized within the distorted wave impulse approximation (DWIA), which will include effects due to final state interaction of outgoing nucleons with the residual nucleus. One advantage of high energy

kinematics of Eq.(7) is the emergence of the eikonal regime in which case FSI effects can be isolated to interfere minimally with the SRC signatures(60, 29).

If now a 2N SRC is probed in $A(e, e', N_f, N_r)X$ reaction the prominent signatures will be that the decay function will exhibit a strong correlation between $\mathbf{p}_i = \mathbf{p}_f - \mathbf{q}$ and \mathbf{p}_r such that

$$\vec{p}_i \approx -\vec{p}_r, \quad (27)$$

if both p_i and $p_f > k_F$. This relation indicates a strong angular correlation between the direction of the yield of recoil nucleons with the direction of the struck nucleon momentum in the initial state.

Such an angular correlation was observed for the first time in the high momentum transfer $p + {}^{12}\text{C} \rightarrow p + p + n + X$ measurement at Brookhaven National Lab's E850 experiment (91, 92). The experiment measured the recoil neutrons produced in coincidence with high energy proton knockout and observed strong back-to-back angular correlation between direction of the measured recoil neutrons and reconstructed momentum of initial bound proton once these momenta exceeded k_F . Remarkably, no correlation was observed when reconstructed momentum $p_i < k_F$.

The existence of such correlations between nucleons in the 2N SRC was confirmed by the JLab, Hall A experiment(21) measuring ${}^{12}\text{C}(e, e', p_f, N_r)$ reaction in which struck proton, p_f has been measured in the coincidence with either recoil proton or neutron, N_r . The kinematics of the experiment were set at $Q^2 \approx 2 \text{ GeV}^2$ and $x \approx 1.2$, with missing momenta in 300–600 MeV/c. With kinematic condition of Eq.(7) satisfied the experiment observed a clear signature for the correlation between the strength of the cross section and the relative angle (γ) of initial, \mathbf{p}_i and recoil nucleon, \mathbf{p}_r momenta.

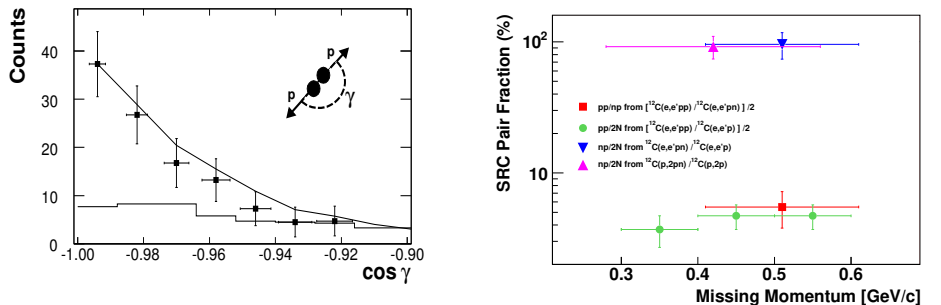


Figure 7: (left panel) The distribution of the cosine of the opening angle between the \vec{p}_i and \vec{p}_r for the $p_i = 0.55 \text{ GeV}/c$ for the ${}^{12}\text{C}(e, e' pp)$ reaction. Figure adapted from Ref.(21). (right panel) The fraction of correlated pair combinations in carbon as obtained from the $A(e, e' pp)$ to $A(e, e' pn)$ reactions (22), as well as from previous $(p, 2pn)$ data (20). Figure adapted from Ref.(22).

Figure 7(left panel) shows the distribution of events in $\cos \gamma$ for the highest p_i setting of 550 MeV/c (21), which is strongly peaked near $\cos \gamma = -1$, corresponding to the back-to-back initial momenta of the struck and recoil protons. The solid curve is the simulated

distribution for scattering from a moving pair, with the pair center-of-mass momentum taken to be a gaussian distribution with a width of 0.136 GeV/c. This width was consistent with the one deduced from the (p, ppn) experiment at BNL (92) as well as with the theoretical calculations(72). Also shown in Fig. 7(left panel) is the angular correlation for the random background as defined by a time window offset from the coincidence peak, which shows the effect of the acceptance of the spectator proton detector.

3.5. Observation of pn Dominance in ^{12}C

In addition to the observation of strong angular correlation between recoil neutron and struck proton momenta emerging from 2N SRCs, the $p+^{12}\text{C} \rightarrow p+p+n+X$ experiment (92) determined that the $(49 \pm 13)\%$ of the events with fast initial protons have correlated backward going fast recoil neutrons.

The theoretical analysis of the above experiment (20), based on the modeling of the nuclear decay function of Eq.26 (93), allowed to relate the above measured event rate to the quantity $P_{pn/pX}$, which represents the probability of finding a pn correlation in the " pX " configuration which contains at least one proton with $p_i > k_{Fermi}$, yielding:

$$P_{pn/pX} = 0.92_{-0.18}^{+0.28}. \quad (28)$$

This result indicates that the removal of a proton from the nucleus with initial momentum 275 – 550 MeV/c, in $\sim 92\%$ of the time, is accompanied by the emission of a correlated neutron that carries momentum roughly equal and opposite to the initial proton momentum.

The BNL experiment did not measure the recoil protons. However the ratio of probabilities of pp and pn SRCs has been estimated in Ref. (20) using the result of Eq.(28), yielding:

$$P_{pp/pX} \leq \frac{1}{2}(1 - P_{pn/pX}) = 0.04_{-0.04}^{+0.09}. \quad (29)$$

One step forward in verifying the above results on probabilities of pn and pp SRCs was the above mentioned Jefferson Lab experiment(21, 22) in which both recoil protons and neutrons have been detected in $^{12}\text{C}(e, e'p, N_r)$ reaction. In this case the experiment measured the fraction of $p_i > k_F$ events in which there was a high-momentum, backward-angle correlated proton or neutron, i.e,

$$R_{pp} = \frac{N(^{12}\text{C}(e, e'p_f p_r))}{N(^{12}\text{C}(e, e'p_f))} \quad \text{and} \quad R_{pn} = \frac{N(^{12}\text{C}(e, e'p_f n_r))}{N(^{12}\text{C}(e, e'p_f))} \quad (30)$$

where $N(\dots)$ stands for the number of events and p_f , p_r and n_r represent struck proton, spectator proton and neutron respectively.

After correcting for the effects of the detector acceptances and neutron efficiency as well as estimating effects due to final state interactions and absorptions of produced nucleons the experiment found(21):

$$R_{pp} = (9.5 \pm 2)\% \quad \text{and} \quad R_{pn} = 96 \pm 22\%. \quad (31)$$

For R_{pp} it was found to be practically independent of p_i in the range of $300 < p_i < 600$ MeV/c, while R_{pn} was estimated for the whole $p_i > 300$ range.

In relation to the BNL experiment one observes remarkable agreement between R_{pn} and $P_{pn/pX}$ (of Eq.(28)), in which both represent the probability of finding a neutron in the pX correlation.

In the estimation of the probability of pp correlation in the JLab measurement, the experiment triggered only on forward $^{12}\text{C}(e,e'p)$ events. Thus the probability of detecting pp pairs was twice that of pn pairs, which indicates that for single pp probability one should compare $P_{pp} = R_{pp}/2$ to the BNL's estimate of $P_{pp/pX}$, again observing very good agreement.

The above estimates result in the following ratio of the probabilities of pp to pn two-nucleons SRCs:

$$\frac{P_{pp}}{P_{pn}} = 0.056_{-0.012}^{+0.021}, \quad (32)$$

which confirms BNL's observation of the strong dominance of pn component in the NN SRCs.

The combined results from BNL and JLab analyses are presented in Fig.7(right panel), which shows very consistent results from BNL and JLab experiments. The fact that these two experiments employing different probes and covering different kinematics in momentum and energy transfer obtained very similar results convincingly indicates that the observed phenomenon is the genuine property of the nuclear ground state.

3.6. Observation of pn Dominance in Heavy Nuclei

The experimental observation of the pn dominance in the ^{12}C nucleus is understood based on the dominance of the tensor interaction in the NN SRC. This fact itself indicates that the above discussed experiments probed NN correlations at internal separations of $\lesssim 1$ Fm. There is rather high confidence in the validity of this conclusion since, as it was discussed in Sec.2.3, the hypothesis of the pn dominance results in two new properties (Eqs.(16) and (17)) of high momentum component of nuclear wave function which are in agreement with the ab-initio variational Monte Carlo calculations of light-nuclei for up to ^{11}B . Thus one will naturally expect that the ^{12}C nucleus being next to ^{11}B , will still exhibit the pn dominance.

If pn dominance is valid also for heavy nuclei it will allow us to extrapolate our results to infinite nuclear matter (32) with rather striking implications for the properties of superdense asymmetric nuclear matter found in the cores of neutron stars. However it is not at all obvious that the phenomenon of pn dominance in NN SRCs will persist for heavy nuclei. For example in the models in which the high momentum component is generated from correlations between nucleons belonging to different nuclear shells it is predicted that for heavy nuclei, with an increase of the number of nucleons the contributions from higher orbitals (shells) will increase, increasing the relative strength of NN SRCs with ($s=0, T=1$) as well as ($s=1, T=1$) and ($s=0, t=0$) spin-isospin combinations(94).

Such an effect can obscure the dominance of the $s = 1, t = 0$ component in the short range NN interaction. Unfortunately one can not unambiguously verify this question theoretically, since VMC calculations are currently applicable for light nuclei only. Other ab-initio calculations that address heavy nuclei does not contain short-range interaction component.

In this respect the experimental verification of the pn dominance in heavy nuclei is significant. Such an analysis of experimental data from JLab was performed in Ref.(23) covering nuclei of ^{12}C , ^{27}Al , ^{56}Fe and ^{208}Pb . The analysis was similar to the one discussed in the above section (21), only that in this case it extracted the double ratios for nuclei A relative to ^{12}C , $[A(e,e'pp)/A(e,e'p)] / [^{12}\text{C}(e,e'pp)/^{12}\text{C}(e,e'p)]$. The data analysis was constrained to the kinematics of $Q^2 \geq 1.5 \text{ GeV}^2$ and $x > 1.2$ and $300 < p_m < 600 \text{ MeV}/c$

thus minimally satisfying condition of Eq.7. Similar to Ref.(21) corrections were made to account for final state interaction and the absorption effects. The final result of the analysis demonstrated that, with the 65% confidence level the pn dominance is observed for all the nuclei consistent with the estimate of Eq.(32).

4. New Directions: Probing Short-Range Correlations in Deep Inelastic Processes

Theoretically, as first discussed in Sec.2.5.1, one can use deep inelastic processes to probe super-fast quarks ($x = \frac{AQ^2}{2M_A q_0} > 1$) in nuclei. With the high energy electron beams that are now available, this is promising new technique for probing nuclear structure at short distances.

4.1. QCD Evolution of Superfast Quarks

One way of probing superfast quarks experimentally is in deep inelastic scattering from nuclei at $x > 1$ (25, 62). The signature that DIS experiments reached the superfast quark regions comes from extracting nuclear partonic distributions that satisfy QCD evolution equations. The first attempt at JLab to reach the superfast region of nuclear partonic distribution was made with a 6 GeV electron beam (95). In this experiment, due to the moderate values of $Q^2 \sim 7 \text{ GeV}^2$, the biggest challenge was to account for the large higher twist as well as finite mass effects. An interesting aspect of the new measurement was how it compared with the earlier measurements from BCDMS/CERN(96) at $\langle Q^2 \rangle \sim 150 \text{ GeV}^2$ and CCFR/FermiLab(97) at $\langle Q^2 \rangle \sim 125 \text{ GeV}^2$ which yielded mutually contradictory results.

The BCDMS collaboration(96) measured nuclear structure function, $F_{2A}(Q^2, x)$ in deep-inelastic scattering of 200 GeV muons from a ^{12}C target extracting data for $\langle Q^2 \rangle = 61 - 150 \text{ GeV}^2$ and $x = 0.85 - 1.15$ ranges. The *per nucleon* F_{2A} has been fitted in the form:

$$F_{2A}(x, Q^2) = F_{2A}(x_0 = 0.75, Q^2)e^{-s(x-0.75)}, \quad (33)$$

with the slope factor estimated as: $s = 16.5 \pm 0.6$. Such an exponent corresponds to a very marginal strength of the high momentum component of the nuclear wave function.

The CCFR collaboration(97) extracted *per nucleon* F_{2A} for ^{56}Fe target measuring neutrino and antineutrino scattering in the charged current sector for $\langle Q^2 \rangle = 125 \text{ GeV}^2$ and $0.6 \leq x \leq 1.2$. The experiment obtained the slope of the x distribution in the form of Eq.(33), with the exponent being evaluated as $s = 8.3 \pm 0.7 \pm 0.7$. This result was in clear contradiction with the BCDMS result, requiring a much too large strength of high-momentum component in the wave function of the ^{56}Fe nucleus. This strength was larger than the one deduced from the quasi-elastic electroproduction in the $x > 1$ region(24, 17, 18, 19, 31, 32).

The existing contradiction can in principle be solved by the JLab experiment if their F_{2A} could be related to the BCDMS and CCFR data by QCD evolution equation. In the JLab experiment (95) the *per nucleon* structure functions F_{2A} have been extracted in the Q^2 (6-9 GeV^2) range for the ^{12}C target. Provided these structure function are corrected for finite target mass and higher twist effects they can be used as an input to the QCD evolution equation to relate them to the structure functions at different Q^2 range. One important feature of the high x kinematics is that, due to the negligible contribution from gluons, the evolution equation for F_{2A} at given Q^2 is fully expressed through the input of

the same structure function measured at different Q^2 , i.e.(98):

$$\begin{aligned} \frac{dF_{2A}(x, Q^2)}{d \log Q^2} = & \frac{\alpha_s}{2\pi} \left\{ 2 \left(1 + \frac{4}{3} \log \left(1 - \frac{x}{A} \right) \right) F_{2,A}(x, Q^2) \right. \\ & \left. + \frac{4}{3} \int_{x/A}^1 \frac{dz}{1-z} \left(\frac{1+z^2}{z} F_{2A} \left(\frac{x}{z}, Q^2 \right) - 2F_{2A}(x, Q^2) \right) \right\}. \end{aligned} \quad (34)$$

In Fig.8(left panel) the results of the evolution of JLab F_{2A} to the region of Q^2 of BCDMS and CCFR experiments are given. Two curves correspond to the two different procedures of the extraction of the leading twist part of the structure function that is used as an input to the evolution equation of Eq.(34). In the one, labelled as F-A evolution, the experimental F_{2A} is corrected for the finite target mass effects according to Ref.(99) and parameterized for fixed $Q^2 = 7 \text{ GeV}^2$ (for details see Ref.(95)). In the second case, labelled as TM+HT evolution, the same JLab data have been analyzed simultaneously for finite target mass and higher twist effects. The finite target mass was accounted for by employing the Nachtmann variable $\xi = 2x/(1 + \sqrt{1 + Q^2/\nu^2})$ while higher twist effects separated through the parameterization of raw data in the form of the inverse powers of Q^2 (for details see Ref.(98)).

As the comparisons with CCFR and BCDMS data in Fig.8(left panel) show, the two inputs predict very similar results in the high Q^2 domain, agreeing better with the CCFR (large high momentum nuclear component case) data for $x \leq 1.05$ and $Q^2 = 125 \text{ GeV}^2$. For $x \sim 1.15$ evolution of JLab structure functions predict a F_{2A} somewhat in between CCFR and BCDMS data. This result indicates that the actual strength of the high momentum component of nuclear wave function is likely larger than BCDMS prediction and smaller than that of CCFR.

Again, it is worth emphasizing that the QCD evolution equation provides the best signature that the DIS process probed the superfast quarks in nuclei and gives completely new tool for probing the strength of the high momentum component of nuclear wave function. By using the evolution equation to relate measurements in different Q^2 domains at $x > 1$, the new JLab 12 GeV data will provide a clear indication whether the deep inelastic scattering has probed superfast quark distributions.

4.2. The Dynamics of the Generation of Superfast Quarks

As discussed above, the onset of the DIS regime in which superfast quarks are probed will result in a unique relation between structure functions F_{2A} measured at different Q^2 regions by the QCD evolution equations.

However, these relations does not allow one to identify the dynamics responsible for the generation of superfast quarks in the nuclear medium. From the discussion of the kinematics of DIS at $x > 1$ in Sec.2.5.1 one observes that with an increase of Q^2 one can reach a domain of incredibly large internal momenta in the nucleus (Fig.3(left panel)). In this respect, one of the main questions is whether the nucleonic degrees of freedom are still relevant for the description of the process. To address this issue one can consider significantly different models in the generation of the superfast quarks and then investigate the feasibility of their experimental verification.

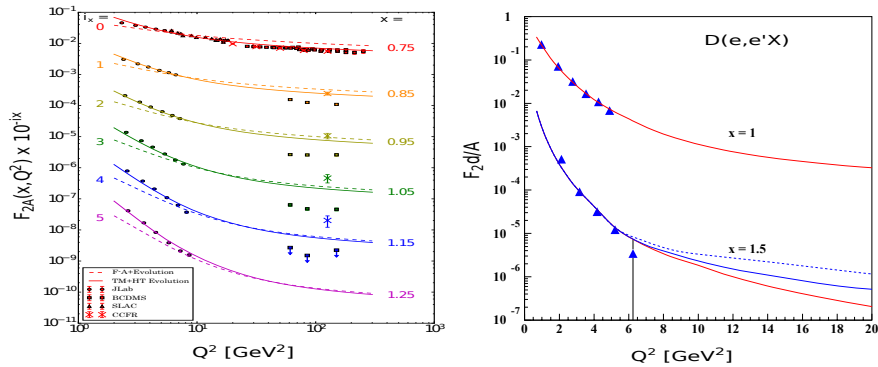


Figure 8: (*left panel*) Comparison of evolution equation results for the *per nucleon* F_{2A} of ^{12}C to experimental measurements. The JLab data are the ones discussed in the text, while details on CCFR, BCDMS and SLAC data are given in Ref.(95). The structure function is multiplied by 10^{-i_x} in order to separate the curves; the values of i_x for each x value are given in the plot. (*right panel*) The DIS structure function of the deuteron is calculated with the convolution model with nucleon modification (lower solid line), with the six-quark model (dotted line) and with the hard gluon exchange model (upper solid line). (The above descriptions are related to the curves labeled by = 1.5). Data are from (68).

4.2.1. Convolution Model. The first most conventional approach is the convolution model. In convolution model it is assumed that the short range correlation of two or more nucleons in the nuclear medium provide sufficient initial momentum to the bound nucleon. These nucleons in turn supply the necessary momentum fraction to the superfast quarks. Within this scenario nucleons retain their degrees of freedom but their structure may be strongly modified. Thus, in this case the nuclear structure function, F_{2A} is expressed through the convolution of structure function of bound nucleon, F_{2N} , and nuclear density matrix, $\rho_d^N(\alpha_i, p_t)$, as follows (25, 62, 100, 65):

$$F_{2A}(x, Q^2) = \sum_N \int_x^2 \rho_d^N(\alpha_i, p_t) \tilde{F}_{2N}\left(\frac{x}{\alpha}, Q^2\right) \frac{d\alpha}{\alpha} d^2 p_t, \quad (35)$$

where α represents the light cone momentum fraction discussed earlier and p_t is the bound nucleon's transverse momentum. The bound nucleon structure function, \tilde{F}_{2N} should account for the nuclear medium modifications in agreement with the EMC effect (see e.g. (25, 100, 65)).

This model can be considered rather conventional since except to the nuclear EMC effect no non-nucleonic degrees of freedom is invoked in the calculation. In addition to the medium modification effects which one expects to be proportional to the internal momentum of the bound nucleon, the short range phenomena here enters through the $\rho_d^N(\alpha_i, p_t)$ function, which contains all the effects of SRCs. The nuclear core effects here enters through the NN potential and one expects that for hard core potentials it will result in the fast vanishing \tilde{F}_{2A} in the $x > 1$ region at large Q^2 .

4.3. Six-Quark Model

Six-quark model is an extreme approach in the description of the evolution of superfast quarks in the nuclear medium in the region of $x \lesssim 2$. In this case one assumes that short-range interaction between six quarks are responsible for the generation of superfast quarks. In the typical diagram the six colinear quarks will exchange five hard gluons transferring the large part of the total momentum fraction to the superfast quark which is subsequently probed by the virtual photon.

In asymptotically large Q^2 and $x \rightarrow 2$ limit, one can deduce the x dependence of the structure function F_{2A} of nuclei using the general quark counting rule (101) according to which:

$$F_{2A}(x)^{6q} \sim (1 - \frac{x}{2})^{10}. \quad (36)$$

It is important to note that in this model one assumes that the large momentum fraction carried by the superfast quark is achieved due to mixing of all six quarks through the exchanges of hard gluons, thus allowing a substantial contribution from the hidden color component of 6q system. In this case however the two nucleon system is totally collapsed into 6q state with complete disappearance of nucleonic degrees of freedom and with no suppression due to the phenomenological hard core repulsion. Thus one expects in this case much softer x dependence of F_{2A} in the $x > 1$ region. In our numerical estimations we use the particular parameterization of 6q model given in Ref.(63).

4.4. Hard Single Gluon Exchange Model

In this model we consider rather intermediate scenario in which large momentum fraction is supplied to the superfast quark not through the mixing of all the six quarks involved in two nucleon system, but just by one hard gluon exchange between the two partons, belonging to two different nucleons. In this model only those diagrams contribute in which the ‘‘communication’’ between two nucleons happens through the single hard gluon exchange between two partons. Such diagrams results in the convolution of two partonic distribution functions, one probed by the external photon and the other by the exchanged hard gluon:

$$F_{2A}(x) \approx N \left[\int \Psi_A(\alpha, p_t) \frac{d\alpha}{\alpha} \frac{d^2 p_t}{2(2\pi)^3} \right]^2 \quad (37)$$

$$\times \int_0^1 \int_0^1 (1 - \frac{x}{y_1 + y_2})^2 \Theta(y_1 + y_2 - x) f_N(y_1) f_N(y_2) dy_1 dy_2,$$

where f_N is the parton distribution function of the nucleon, and y_1 and y_2 represent the momentum fractions of partons, one from each nucleon, participating in the hard scattering. In this model some of the effects of short range repulsion will be present in the non-perturbative dynamics of parton distribution function of the nucleon. In the asymptotically high Q^2 and $x \rightarrow 2$ the model has the parametric form of the 6q model due to the $(1 - y)^3$ dependence of the nucleon PDFs.

In summary we present three different scenarios how the super fast quarks can be generated in the NN system. The best way of checking it experimentally is using the deuteron target, since for heavy nuclei multi-nucleon SRCs might contribute strongly masking the effects due to the NN interaction at the core.

In Fig.8(right panel) we present the predictions of above discussed models for the structure function of the deuteron at $x = 1$ and $x = 1.5$. These estimates show the real possibility for discriminating between different scenarios of the interaction at core distances in the future experiment with 12 GeV Jefferson Lab.

Extending the above discussion to heavy nuclei it is worth mentioning that in addition to the question how the transition from NN system to quark configuration happens one need to address the question of the 3N- and higher order SRCs. An interesting implication of the role of the 3N SRCs in the DIS regime is that if one considers the ratio of cross sections similar to Fig.4 in $1 < x < 2$ region the plateau will disappear with the increase of Q^2 . The observation of

such an effect is due to the fact that with an increase of Q^2 in the DIS regime the internal momenta steeply increase at fixed x (Eq.(23)) as a result even for $x < 2$ one should expect substantial contribution due to 3N SRCs which will disrupt the plateau observed experimentally in the quasi-elastic kinematics.

5. Conclusion and Outlook

We have reviewed the recent progress in studies of short range correlations in nuclei that has been driven by a the series of high energy experiments with proton and electron probes. We demonstrated how the inclusive electronuclear processes in the $x > 1$ quasi-elastic region were able to identify NN short range correlations in nuclei and extract the parameter $a_2(A, Z)$ that characterizes the strength of NN SRCs in the high momentum part of the nuclear wave functions. We discuss the observation of apparent correlation between the strength of the medium modification of partonic distributions in nuclei and the $a_2(A, z)$ factor of 2N SRCs.

For the triple-coincident experiments, we reviewed the observed strong angular correlation between the constituents of 2N SRCs and the strong dominance of the pn component in these correlations. The pn dominance is understood based on the large tensor interaction in the NN SRCs at $\lesssim 1$ fm distances. We reviewed the implication of this dominance on the properties of the high momentum distribution of nucleons in nuclei and recent observations which apparently are in agreement with these properties.

The next subject of the review was the physics of the three-nucleon correlations where the current results are rather inconclusive. We show that in order to make a definitive probe of the three-nucleon correlations one needs considerably higher Q^2 which can be reached in upcoming experiments at Jefferson Lab.

Finally, we review the new and promising direction of studying short range properties of nuclei at core distances with deep inelastic scattering at Bjorken $x > 1$ region. We reviewed the first such experiment completed at Jefferson Lab and demonstrated its potential in verifying the validity of QCD evolution equation for such superfast quarks. We discussed also the sensitivity of the cross section of inclusive scattering from the superfast quarks to the particular mechanism of NN interaction at core distances.

Future experiments at JLab, as well as at high energy labs such as LHC, JPARC and possibly EIC, might provide significant new information about the dynamics of NN interactions at the core.

ACKNOWLEDGMENTS

* During the writing of this manuscript, our good friend and co-author Patricia Solvignon passed away. Though very young, Patricia had already had made quite an impact in the field of nuclear physics and had several approved experiments at Jefferson Lab to measure the effects of short-range correlations in nuclei. In fact, Patricia was a spokesperson on several of the past and future Jefferson Lab experiments described herein. Patricia was a good friend and an outstanding scientist and will be sorely missed.

This work is supported by the U.S. Department of Energy, Office of Science, Office of Nuclear Physics grants under contracts de-sc0013615, DE-AC05-06OR23177, and DE-FG02-01ER-41172. We are thankful to our colleagues for collaboration and assistance in performing the above described research in general and preparation of the current article in particular.

LITERATURE CITED

1. Machleidt R, Sammarruca F. *Phys. Scripta* 91:083007 (2016)
2. Lapikas L, et al. *Phys. Rev.* C61:064325 (2000)
3. Jastrow R. *Phys. Rev.* 98:1479 (1955)
4. Bethe HA. *Ann. Rev. Nucl. Part. Sci.* 21:93 (1971)
5. Amado RD. *Phys. Rev.* C14:1264 (1976)
6. Brueckner KA, Eden RJ, Francis NC. *Phys. Rev.* 98:1445 (1955)
7. Rock S, et al. *Phys. Rev. Lett.* 49:1139 (1982), [424(1982)]
8. Arnold RG, et al. *Phys. Rev. Lett.* 61:806 (1988)
9. Rock S, et al. *Phys. Rev.* D46:24 (1992)
10. Day D, et al. *Phys. Rev. Lett.* 43:1143 (1979)
11. Rock S, et al. *Phys. Rev.* C26:1592 (1982)
12. Day DB, et al. *Phys. Rev. Lett.* 59:427 (1987)
13. Royer D, et al. *Phys. Rev.* C12:327 (1975)
14. Marchand C, et al. *Phys. Rev. Lett.* 60:1703 (1988), [Erratum: *Phys. Rev. Lett.* 60,2704(1988)]
15. Alanakian KV, et al. *Phys. Atom. Nucl.* 60:1069 (1997), [*Yad. Fiz.* 60,1194(1997)]
16. Alanakian KV, et al. *Phys. Atom. Nucl.* 61:207 (1998), [*Yad. Fiz.* 61,256(1998)]
17. Egiyan KS, et al. *Phys. Rev. C* 68:014313 (2003)
18. Egiyan KS, et al. *Phys. Rev. Lett.* 96:082501 (2006)
19. Fomin N, et al. *Phys. Rev. Lett.* 108:092502 (2012)
20. Piasezky E, et al. *Phys. Rev. Lett.* 97:162504 (2006)
21. Shneor R, et al. *Phys. Rev. Lett.* 99:072501 (2007)
22. Subedi R, et al. *Science* 320:1476 (2008)
23. Hen O, et al. *Science* 346:614 (2014)
24. Frankfurt LL, Strikman MI, Day DB, Sargsian M. *Phys. Rev. C* 48:2451 (1993)
25. Frankfurt LL, Strikman MI. *Phys. Rept.* 160:235 (1988)
26. Seely J, et al. *Phys. Rev. Lett.* 103:202301 (2009)
27. Weinstein LB, et al. *Phys. Rev. Lett.* 106:052301 (2011)
28. Arrington J, et al. *Phys. Rev.* C86:065204 (2012)
29. Sargsian MM, Abrahamyan TV, Strikman MI, Frankfurt LL. *Phys. Rev. C* 71:044615 (2005)
30. Schiavilla R, Wiringa RB, Pieper SC, Carlson J. *Phys. Rev. Lett.* 98:132501 (2007)
31. Sargsian MM. *Phys. Rev.* C89:034305 (2014)
32. McGauley M, Sargsian MM arXiv:1102.3973 [nucl-th] (2011)
33. Wiringa RB, Schiavilla R, Pieper SC, Carlson J. *Phys. Rev.* C89:024305 (2014)
34. Ryckebusch J, Cosyn W, Vanhalst M. *J. Phys.* G42:055104 (2015)

35. Boeclin WU, et al. *Phys. Rev. Lett.* 107:262501 (2011)
36. Hen O, Miller GA, Piasetzky E, Weinstein LB arXiv:1611.09748 [nucl-ex] (2016)
37. Alvioli M, Ciofi degli Atti C, Morita H. *Phys. Rev.* C94:044309 (2016)
38. Chen JW, Detmold W, Lynn JE, Schwenk A arXiv:1607.03065 [hep-ph] (2016)
39. Boeclin W, Sargsian M. *Int. J. Mod. Phys.* E24:1530003 (2015)
40. Neff T, Feldmeier H, Horiuchi W. *Phys. Rev.* C92:024003 (2015)
41. Ciofi degli Atti C. *Phys. Rept.* 590:1 (2015)
42. Cai BJ, Li BA. *Phys. Rev.* C93:014619 (2016)
43. Furnstahl RJ, Hebeler K. *Rept. Prog. Phys.* 76:126301 (2013)
44. Weiss R, et al. arXiv:1612.00923 [nucl-th] (2016)
45. Ciofi degli Atti C, Mezzetti CB, Morita H arXiv:1701.08211 [nucl-th] (2017)
46. Frankfurt LL, Strikman MI. *Phys. Rept.* 76:215 (1981)
47. Weinberg S. *Phys. Rev.* 150:1313 (1966)
48. Feynman R. P. *Photon-hadron interactions* (1973)
49. Sargsian MM. *Int. J. Mod. Phys.* E10:405 (2001)
50. Frankfurt LL, Sargsian MM, Strikman MI. *Phys. Rev.* C56:1124 (1997)
51. Sargsian MM. *Phys. Rev.* C82:014612 (2010)
52. Lepage GP, Brodsky SJ. *Phys. Rev.* D22:2157 (1980)
53. Miller GA. *Prog. Part. Nucl. Phys.* 45:83 (2000)
54. Nogga A, Kamada H, Gloeckle W. *Nucl. Phys.* A689:357 (2001)
55. Wiringa RB, Stoks VGJ, Schiavilla R. *Phys. Rev.* C51:38 (1995)
56. Moniz EJ, et al. *Phys. Rev. Lett.* 26:445 (1971)
57. Artiles O, Sargsian MM. *Phys. Rev.* C94:064318 (2016)
58. Frankfurt L, Sargsian M, Strikman M. *Int. J. Mod. Phys.* A23:2991 (2008)
59. Freese AJ, Sargsian MM, Strikman MI. *Eur. Phys. J.* C75:534 (2015)
60. Sargsian MM, Abrahamyan TV, Strikman MI, Frankfurt LL. *Phys. Rev.* C71:044614 (2005)
61. Aubert JJ, et al. *Phys. Lett.* B105:315 (1981)
62. Sargsian MM, et al. *J. Phys.* G29:R1 (2003)
63. Carlson CE, Lassila KE. *Phys. Rev.* C51:364 (1995)
64. Sargsian MM. *Nucl. Phys.* A782:199 (2007)
65. Melnitchouk W, Sargsian M, Strikman MI. *Z. Phys.* A359:99 (1997)
66. Cosyn W, Sargsian M. *Phys. Rev.* C84:014601 (2011)
67. Arrington J, et al. *Phys. Rev.* C53:2248 (1996)
68. Arrington J, et al. *Phys. Rev. Lett.* 82:2056 (1999)
69. Arrington J, et al. *Phys. Rev.* C64:014602 (2001)
70. Korover I, et al. *Phys. Rev. Lett.* 113:022501 (2014)
71. Egiyan KS, et al. *Phys. Rev. Lett.* 98:262502 (2007)
72. Ciofi degli Atti C, Simula S. *Phys. Rev.* C53:1689 (1996)
73. Higinbotham DW, Hen O. *Phys. Rev. Lett.* 114:169201 (2015)
74. Gomez J, et al. *Phys. Rev.* D49:4348 (1994)
75. Adams MR, et al. *Z. Phys.* C65:225 (1995)
76. Amaudruz P, et al. *Nucl. Phys.* B441:3 (1995)
77. Geesaman DF, Saito K, Thomas AW. *Ann. Rev. Nucl. Part. Sci.* 45:337 (1995)
78. Malace S, Gaskell D, Higinbotham DW, Cloet I. *Int. J. Mod. Phys.* E23:1430013 (2014)
79. Higinbotham D, Miller GA, Hen O, Rith K. *CERN Cour.* 53N4:24 (2013)
80. Hen O, et al. *Int. J. Mod. Phys.* E22:1330017 (2013)
81. Hen O, Piasetzky E, Weinstein L. *Phys. Rev. C* 85:047301 (2012)
82. Ducret J, et al. *Phys. Rev.* C49:1783 (1994)
83. Blomqvist KI, et al. *Phys. Lett.* B424:33 (1998)
84. Ulmer PE, et al. *Phys. Rev. Lett.* 89:062301 (2002)
85. Benmokhtar F, et al. *Phys. Rev. Lett.* 94:082305 (2005)

86. Rvachev M, et al. *Phys.Rev.Lett.* 94:192302 (2005)
87. Boeglin WU, et al. arXiv:1410.6770 [nucl-ex] (2014)
88. Passchier I, et al. *Phys. Rev. Lett.* 88:102302 (2002)
89. Mayer M arXiv:1610.06109 [nucl-ex] (2016)
90. Mihovilovic M, et al. *Phys. Rev. Lett.* 113:232505 (2014)
91. Aclander JLS, et al. *Phys. Lett.* B453:211 (1999)
92. Tang A, et al. *Phys. Rev. Lett.* 90:042301 (2003)
93. Yaron I, et al. *Phys. Rev.* C66:024601 (2002)
94. Alvioli M, et al. *Phys. Rev.* C87:034603 (2013)
95. Fomin N, et al. *Phys. Rev. Lett.* 105:212502 (2010)
96. Benvenuti AC, et al. *Z. Phys.* C63:29 (1994)
97. Vakili M, et al. *Phys. Rev.* D61:052003 (2000)
98. Freese AJ, Sargsian MM arXiv:1511.06044 [hep-ph] (2015)
99. Schienbein I, et al. *J. Phys.* G35:053101 (2008)
100. Sargsian MM, Simula S, Strikman MI. *Phys. Rev.* C66:024001 (2002)
101. Brodsky SJ, Farrar GR. *Phys. Rev. Lett.* 31:1153 (1973)